











 Cite this: *Nanoscale*, 2024, **16**, 8132

## Toward the nanoscale chemical and physical probing of milk-derived extracellular vesicles using Raman and tip-enhanced Raman spectroscopy†

 Luca Buccini, <sup>‡a</sup> Anacleto Proietti, <sup>‡a</sup> Giancarlo La Penna, <sup>a</sup>  
 Chiara Mancini, <sup>a</sup> Francesco Mura, <sup>a,b</sup> Stefano Tacconi, <sup>c</sup> Luciana Dini, <sup>c</sup>  
 Marco Rossi <sup>a,b</sup> and Daniele Passeri <sup>\*a,b</sup>

Tip-enhanced Raman spectroscopy (TERS) is an advanced technique to perform local chemical analysis of the surface of a sample through the improvement of the sensitivity and the spatial resolution of Raman spectroscopy by plasmonic enhancement of the electromagnetic signal in correspondence with the nanometer-sized tip of an atomic force microscope (AFM). In this work, TERS is demonstrated to represent an innovative and powerful approach for studying extracellular vesicles, in particular bovine milk-derived extracellular vesicles (mEVs), which are nanostructures with considerable potential in drug delivery and therapeutic applications. Raman spectroscopy has been used to analyze mEVs at the micrometric and sub-micrometric scales to obtain a detailed Raman spectrum in order to identify the 'signature' of mEVs in terms of their characteristic molecular vibrations and, therefore, their chemical compositions. With the ability to improve lateral resolution, TERS has been used to study individual mEVs, demonstrating the possibility of investigating a single mEV selected on the surface of the sample and, moreover, analyzing specific locations on the selected mEV with nanometer lateral resolution. TERS potentially allows one to reveal local differences in the composition of mEVs providing new insights into their structure. Also, thanks to the intrinsic properties of TERS to acquire the signal from only the first few nanometers of the surface, chemical investigation of the lipid membrane in correspondence with the various locations of the selected mEV could be performed by analyzing the peaks of the Raman shift in the relevant range of the spectrum (2800–3000 cm<sup>-1</sup>). Despite being limited to mEVs, this work demonstrates the potential of TERS in the analysis of extracellular vesicles.

Received 28th February 2024,

Accepted 20th March 2024

DOI: 10.1039/d4nr00845f

[rsc.li/nanoscale](https://rsc.li/nanoscale)

## Introduction

Milk is an essential resource for human nutrition, with numerous bioactive compounds such as proteins, amino acids and growth and immunological factors.<sup>1</sup> In recent years, it has been shown that milk, especially bovine milk, is rich in extracellular vesicles (EVs), which are nano- to micrometer-sized structures released from the cell into the extracellular space and play a very important role in cell–cell communication and

numerous biological processes.<sup>2,3</sup> The high bioavailability and the ability to cross biological barriers are some of the characteristics of mEVs that make them highly promising for drug delivery and theranostic applications.<sup>4,5</sup> As a consequence of the increasing interest in EVs, a variety of analytical techniques have been employed to extensively study them, in order to gain a comprehensive overview of their morphology, functionality, and chemical composition.<sup>6,7</sup> Raman spectroscopy is a non-destructive technique which can provide a unique fingerprint of the chemical composition of a sample through the analysis of molecular vibrational modes. The Raman spectrum is obtained when the sample is irradiated with a monochromatic laser and contains all the characteristic peaks corresponding to the vibrational frequencies of the molecules present on the sample. In particular, Raman spectroscopy on EVs can identify proteins, lipids and nucleic acids.<sup>8,9</sup> In numerous works, Raman spectroscopy has been used to assess the purity of EV preparations<sup>10,11</sup> or to detect biomarkers under pathological conditions.<sup>12,13</sup> Despite its unique features, the main limit-

<sup>a</sup>Department of Basic and Applied Sciences for Engineering, Sapienza University of Rome, Via A. Scarpa 14, 00161 Rome, Italy. E-mail: [daniele.passeri@uniroma1.it](mailto:daniele.passeri@uniroma1.it)
<sup>b</sup>Research Center for Nanotechnology Applied to Engineering of Sapienza University of Rome (CNIS), Piazzale A. Moro 5, 00185 Rome, Italy

<sup>c</sup>Department of Biology and Biotechnology "C. Darwin", Sapienza University of Rome, 00185 Rome, Italy

† Electronic supplementary information (ESI) available. See DOI: <https://doi.org/10.1039/d4nr00845f>

‡ These authors contributed equally to this work.



ation of Raman spectroscopy is represented by the size of the spot of the laser, which hampers the use of this technique in the analysis of nanoscale materials, and its sensitivity, which requires a sufficient volume of the sample to produce a detectable signal. Tip-enhanced Raman spectroscopy (TERS) is an advanced technique that combines Raman spectroscopy with atomic force microscopy (AFM) in order to increase the spatial resolution and sensitivity of Raman spectroscopy. In TERS, the presence of a metallic coating on the tip and its nanometer size result in the amplification of the Raman signal through a plasmonic effect.<sup>14</sup> This allows the acquisition of Raman spectra from nanosized volumes of the samples enabling their nanoscale chemical analysis.<sup>15</sup> TERS has been used to study nuclear acids, proteins, lipid membranes and cells.<sup>16–18</sup> Through TERS, it is possible to achieve optimal spatial resolution for the study of biological samples, which would allow understanding and analysis at the molecular level, while standard Raman spectroscopy enables only the investigation of bulk samples.<sup>19</sup> In a recent study, TERS was performed on micrometer extracellular vesicles released from red blood cells, suggesting that this technique is promising for investigating the molecular heterogeneity of the surface of EVs.<sup>20</sup> In this work, we demonstrated the potentiality of TERS to obtain detailed local information on nanometer-sized mEVs, which can be eventually used to obtain a complete biochemical characterization and a comprehensive view of the specific molecular vibrations of the bonds present on the sample. After a preliminary characterization of the mEVs using AFM and transmission electron microscopy (TEM), conventional Raman spectra of the mEV films were collected and analyzed in order to obtain their ‘vibrational signature’. Finally, TERS was used to obtain the Raman spectra of the isolated mEVs. Also, different locations on the surface of an isolated mEV were selected and probed to retrieve information about the compositional variations on the membrane, which paves the way to the nanoscale chemical mapping of the surface of a single mEV.

## Materials and methods

### mEV isolation

Preparation and isolation of mEVs from bovine milk collected from a local farm (Rome, Italy) were performed following methodologies already described in the literature.<sup>21–24</sup> After verifying the quality of isolation using standard western blot techniques, mEVs were preserved for subsequent TEM and AFM analyses by immersing them in 0.1% paraformaldehyde (PFA) in PBS for 30 minutes at room temperature.

### Transmission electron microscopy

For TEM analysis, the preserved mEVs were stained with 2% uranyl acetate for 10 minutes and placed on carbon-coated grids with a mesh size of 200 for observation. The analysis was performed using a JEM-F200 multi-purpose electron microscope (JEOL, Japan) operating at 80 keV. TEM of mEVs was performed using ImageJ and statistical analysis was performed on no less than 200 mEVs.

### Atomic force microscopy

For AFM analysis, the preserved mEVs were diluted with water and deposited on a calcium fluoride slide (Crystran Ltd, UK). AFM topographical images were acquired in standard contact mode with DNP tips, with a spring constant of 0.06 (N m<sup>-1</sup>) (Bruker Inc.) with a Cypher Video-Rate AFM (Oxford Instruments, UK). The software Gwyddion (<https://www.gwyddion.net>) was used to analyze the obtained images. To reduce inaccuracies caused by temperature drifting and sample tilting, the pictures underwent minimum processing such as deleting line coupling, compensating for substrate tilting, and removing a mean plane. Using Gwyddion’s segmentation tools, statistical analysis on the number and size of the isolated mEVs was performed on no less than 200 isolated mEVs.

### Raman spectroscopy

The mEVs were analyzed using a confocal inVia™ Raman spectrometer (Renishaw, UK), with a 250 mm focal length. 5 μL of mEV suspension was deposited on a calcium fluoride slide (Crystran Ltd, UK) and left to dry in air. They were analyzed at room temperature in the 600–3200 cm<sup>-1</sup> spectral range. The signal was dispersed by a holographic grating of 1800 lines per mm and collected using a Peltier-cooled CCD detector. The excitation line at 532.1 nm was produced by a Nd:YAG continuous-wave diode-pumped solid-state laser (Renishaw) and focused on the sample through a short distance working objective N PLAN 50×, with NA = 0.75 (Leica Microsystems).

### Tip-enhanced Raman spectroscopy

TERS characterization was performed using a Renishaw inVia™ confocal Raman spectrometer with 250 mm focal length and a Mitutoyo 50× magnification objective (NA 0.42 M PLAN, APO SL type, WD 0.5 mm) coupled to a Bruker Innova™ AFM.<sup>25</sup> The excitation line is the same as that used for Raman analysis (λ = 532.1 nm). TERS tips (Next-Tip S.L.) consisted of commercial AFM tips with an elastic constant of 45 N m<sup>-1</sup> and a nominal resonance frequency of 335 kHz, on which Ag and Au nanoparticles were deposited upon ultra-high vacuum conditions with a final curvature radius of 5 nm.

## Results and discussion

### Preliminary characterization of mEVs

Preliminary characterization of mEVs was performed to assess their dimensions and size distribution. Fig. 1(a) shows two typical TEM images which confirmed that mEVs have a spherical shape. The statistical analysis on size distribution, reported in Fig. 1(b), indicated an average size of 86 ± 34 nm. Analogous analysis of the AFM images, a typical of which is reported in Fig. 1(c), gave a result of 94 ± 38 nm, in very good agreement with the TEM results. Both TEM and AFM results demonstrated that mEVs were monodisperse and confirmed their structural integrity and purity.



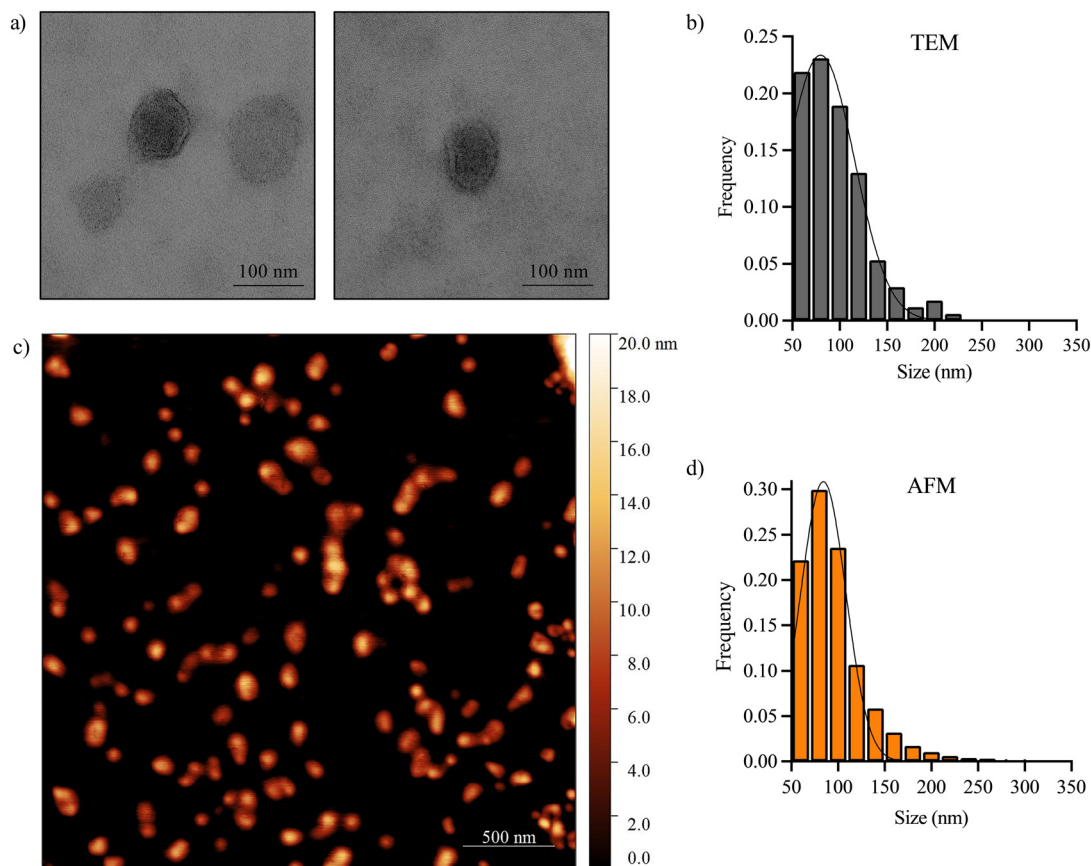


**Fig. 1** Morphological characterization of milk-derived extracellular vesicles: (a) typical TEM images of mEVs and (b) statistics of their size on the basis of TEM analyses; (c) typical AFM image of mEVs and (d) statistics of their size on the basis of AFM analysis.

### Raman spectroscopic analysis on mEVs

Raman analysis of mEVs was performed by collecting the spectra in two typical spectral range regions of biological structures, *i.e.*, 600–1800  $\text{cm}^{-1}$  and 2600–3200  $\text{cm}^{-1}$ . In order to have a sufficient amount of sample, the area of interest was selected on the ‘coffee ring’ resulting at the borders of the drop on the substrate. Acquisitions were repeated at several hundred different points in the same region to confirm reproducibility. The characteristic peaks of the Raman bands are shown in Fig. 2, which was obtained using the 532.1 nm excitation wavelength with a laser power of 50 mW, 1 s of exposure time, and 2 accumulations. As for the peaks in the 600–1800  $\text{cm}^{-1}$  region, these include the peak at 1003  $\text{cm}^{-1}$  for phenylalanine and the peak at 1064  $\text{cm}^{-1}$  assigned to the C–C stretching in lipids. The 1126  $\text{cm}^{-1}$  and 1263  $\text{cm}^{-1}$  peaks correspond to C–N stretching and amide III in proteins, respectively. Additionally, the peak at 1296  $\text{cm}^{-1}$  is related to  $\text{CH}_2$  deformation in lipids, while the peak at 1440  $\text{cm}^{-1}$  is assigned to  $\text{CH}_2$  and  $\text{CH}_3$  deformation in lipids and proteins. Finally, the peak at 1655  $\text{cm}^{-1}$  represents amide I and C=C bond stretching in acyl chains. In addition, other peaks of lower intensities were identified, including 718  $\text{cm}^{-1}$  with 876  $\text{cm}^{-1}$  assigned to symmetric and asymmetric stretching of the choline  $\text{N}^+(\text{CH}_3)_3$  group, the peak at 1740  $\text{cm}^{-1}$  for (C=O)

ester stretching present in lipids, and the peak at 1522  $\text{cm}^{-1}$  for carotenoids. As for the peaks in the 2600–3200  $\text{cm}^{-1}$  region, these include those at 2850  $\text{cm}^{-1}$  and 2882  $\text{cm}^{-1}$ , which represent symmetric and asymmetric  $\text{CH}_2$  stretching in lipids, and the peak at 2930  $\text{cm}^{-1}$ , which is related to the symmetric  $\text{CH}_3$  stretching of proteins and lipids. The complete peak assignment is reported in Table 1. The identified peaks are in agreement with the outcomes of previous Raman studies on extracellular vesicles.<sup>26–32</sup> This establishes a Raman fingerprint to be used as a reference for the subsequent TERS analysis.

### Tip-enhanced Raman spectroscopic analysis on mEVs

TERS analyses were first performed in the same region on the coffee ring area obtaining the different characteristic peaks of the Raman bands at low and high wavenumbers. First of all, tip-in and tip-out spectra were acquired. This is a standard procedure when carrying out TERS measurements in order to assess the actual amplification that can be obtained. Basically, this procedure consists of conducting a measurement in which the tip is very close to the sample so that the plasmonic effect amplifies the signal<sup>33</sup> (tip-in measurement) and then comparing it with a measurement in which the tip is very far away (ideally infinitely far from the sample) so that there is no



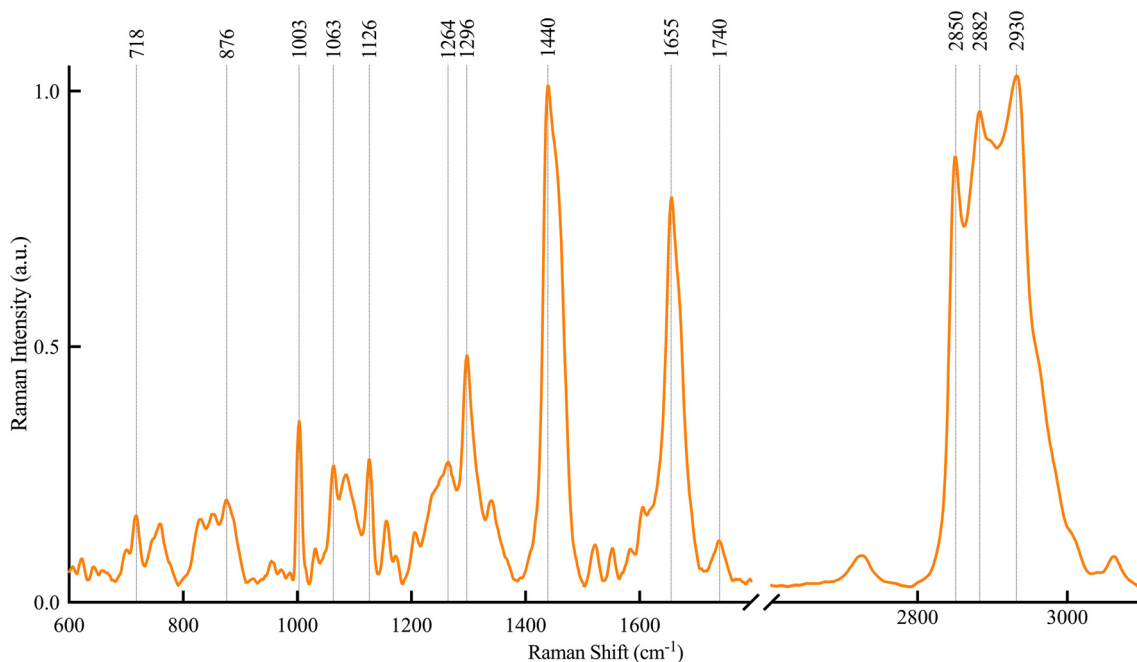


**Fig. 2** Standard Raman spectrum of mEVs obtained by averaging hundreds of acquisitions in correspondence with the border of the sample droplet on the substrate ('coffee ring').

**Table 1** Summary of the identified peaks and bands in the standard Raman spectrum with their assignments according to the data reported in the literature<sup>26–32</sup>

#### Assignments of Raman peaks

Position (cm <sup>-1</sup> )	Component
701	Cholesterol
718	Symmetric stretching of the choline N <sup>+</sup> (CH <sub>3</sub> ) <sub>3</sub> group
759	Tryptophan
876	Asymmetric stretching of the choline N <sup>+</sup> (CH <sub>3</sub> ) <sub>3</sub> group
1003	Phenylalanine
1064	C–C stretching in lipids
1126	C–N stretching
1263	Amide III
1296	CH <sub>2</sub> deformation in lipids
1440	CH <sub>2</sub> and CH <sub>3</sub> deformation
1522	Carotenoids
1655	Amide I and C=C bond stretching in acyl chains
1740	(C=O) ester stretching
2850	Symmetric CH <sub>2</sub> stretching
2882	Asymmetric CH <sub>2</sub> stretching
2930	Symmetric CH <sub>3</sub> stretching

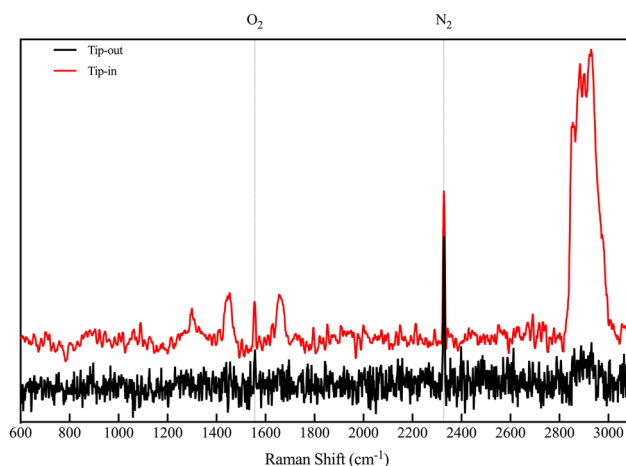


**Fig. 3** Example of the comparison of TERS tip-in and tip-out measurements performed on the coffee ring in a typical TERS experiment.

amplification effect (tip-out measurement). By comparing these two measurements it is possible to understand which and how much signal is being amplified by the TERS effect and how much is a residual of the classical Raman signal. A typical result is reported in Fig. 3, which shows that the peaks present at 1556 cm<sup>-1</sup> and 2328 cm<sup>-1</sup> are not related to the TERS measurement but to a residual of the Raman signal. In particular, they are attributable to the gaseous components present in the atmosphere (O<sub>2</sub> and N<sub>2</sub>, respectively). These artifacts are present due to the long working distance of the objec-

tive and, although they do not represent interesting signals for characterization purposes, they can be used as indicators of the correctness of the measurement itself. In a typical TERS experiment, the topography of the sample is first acquired in order to collect the image of the surface where the locations of interest for the Raman investigation are selected.

The same area of the coffee ring has been used to acquire multiple TERS spectra in order to assess the repeatability of the method. Indeed, while in 'macroscale' methods the evaluation of repeatability can be considered a well-established procedure, in nanoscale techniques its assessment may be quite



an issue and requires some specific attention. In particular, TERS spectra were acquired at almost the same point after a fixed time (*e.g.*, approximately one hour). In order to have a good signal-to-noise ratio (SNR), to avoid fluctuations due to drifting, for the modulation of the chemical properties of the surface at the nanometer scale, and for possible modifications induced by laser irradiation, repeatability tests were performed on different (but close) locations of the coffee ring. The choice of the coffee ring instead of a single EV allowed us to have a significant amount of material from extracellular vesicles so that the average spectrum is obtained, thus avoiding the local fluctuations due to nanoscale non-homogeneity of the chemical properties of the EV membrane. Also, this allowed us to probe different points which have the same average properties but are sufficiently far from each other, so that each measurement is not affected by the possible modification of the sample due to local heating produced by exposure to laser irradiation. An example of two TERS spectra acquired following this procedure is reported in Fig. S1.† The two spectra were collected using different numbers of accumulations (*i.e.*, 2 and 4 subsequent TERS spectra). Notably, spectra collected with an increased number of accumulations did not show changes in the spectral content in terms of detected peaks, but only an increase in the SNR, as expected. Therefore, the number of accumulations has been kept as low as possible (but always at least 2) to avoid excessive heating of the sample and tip. Fig. S2† shows a magnified image of the spectra acquired in the region of main interest for the present work (2800–3100  $\text{cm}^{-1}$ ). The two measurements definitely do not show any significant difference – with the exception, obviously, of a higher SNR in correspondence with a higher number of accumulations. Thus, repeated TERS measurements on the same sample acquired after a relatively short time present the very same peaks, confirming the repeatability of our TERS measurements. However, the issue of the repeatability of TERS measurements at the nanoscale requires further discussion. First of all, nanoscale characterization is in principle able to detect variations at the nanometer scale on the sample surface. Therefore, in order to assess the repeatability of the measurements at the nanometer scale, careful control and evaluation of instrumental drift must be carried out. A second point which must be considered is that all TERS spectra were obtained by selecting a certain number of accumulations. The higher the number of accumulations, the higher the SNR. Nevertheless, a larger number of accumulations require a longer acquisition time, during which the laser illuminates the sample increasing the risk of thermal degradation of the sample itself. For the sake of completeness, it must also be noted that prolonged exposure to the laser radiation may also degrade the coating of the tip, which results in a variation of the performance of the tip and, definitely, in the outcome of TERS measurements. Therefore, a reasonable compromise must be selected. The last point which must be considered when evaluating the repeatability of TERS – especially on biological samples – is the effect of heating and thermal degradation of the sample. When multiple spectra are acquired at

the same point on the surface, local heating may occur modifying the local chemical properties and thus introducing artifacts into the TERS spectra. While this is generally important in Raman spectroscopy, it may be extremely relevant in TERS where laser-induced heating effects can be particularly intense due to the highly confined electromagnetic field at the sample surface.<sup>16</sup>

A typical TERS spectrum, as reported in Fig. 4, which was obtained with 25 mW power, 10 s exposure time, and 2 accumulations, shows clear peaks in the same two Raman bands which can be easily rationalized also on the basis of the standard Raman spectra previously acquired. For instance, in the range of 600–1800  $\text{cm}^{-1}$ , the peaks at 702  $\text{cm}^{-1}$  and 876  $\text{cm}^{-1}$  represent the characteristic peaks of cholesterol and asymmetric stretching of choline, respectively. The peaks at 1064  $\text{cm}^{-1}$  and 1296  $\text{cm}^{-1}$  are related to C–C stretching and  $\text{CH}_2$  deformation in lipids. Furthermore, two distinct bands relating to the peaks 1440  $\text{cm}^{-1}$  and 1455  $\text{cm}^{-1}$  were detected, which represent the scissoring and bending of  $\text{CH}_2$  and  $\text{CH}_3$ . Other peaks at 1652  $\text{cm}^{-1}$  and 1665  $\text{cm}^{-1}$  can be attributed to the acyl chains and amide I. As for the 2600–3200  $\text{cm}^{-1}$  Raman shift region, there are characteristic peaks that identify proteins and lipids, *i.e.*, the symmetric and asymmetric  $\text{CH}_2$  stretching at 2850  $\text{cm}^{-1}$  and 2882  $\text{cm}^{-1}$ , respectively, and the peak at 2930  $\text{cm}^{-1}$  is attributed to the symmetric  $\text{CH}_3$  stretching. In this region, two other peaks related to 2900  $\text{cm}^{-1}$  and 2921  $\text{cm}^{-1}$  are also identifiable which fall within the general band of the CH stretching mode. As can be seen in the spectrum obtained in the TERS configuration, some peaks differ in intensity and width from those obtained in standard Raman spectra. Indeed, in the range 600–1800  $\text{cm}^{-1}$  almost all the peaks obtained in the Raman spectra were obtained, even if with lower intensity. In particular, in the region 1400–1800  $\text{cm}^{-1}$  some very distinct and close peaks were observed such as 1440  $\text{cm}^{-1}$  and 1456  $\text{cm}^{-1}$  or 1652  $\text{cm}^{-1}$  and 1665  $\text{cm}^{-1}$ , which are not resolved with standard Raman spectroscopy. Furthermore, in the high Raman shift region, the same information and peaks present in standard Raman spectroscopy (2850  $\text{cm}^{-1}$ , 2882  $\text{cm}^{-1}$  and 2930  $\text{cm}^{-1}$ ) were collected, but with two additional peaks (2900  $\text{cm}^{-1}$  and 2921  $\text{cm}^{-1}$ ), which confirms the possibility to recognize major CH vibrational bonds present in mEVs.

It is worth noting that, as clearly seen in the presented Raman and TERS spectra, a confocal Raman signal has undoubtedly a much higher SNR than that in TERS. This is due to the fact that the signal is collected from a bigger volume of material, which is proportional to the area illuminated by the electromagnetic radiation, *i.e.*, to the spot of the laser which is approximately 1  $\mu\text{m}$ . As a direct consequence, the main drawback of standard confocal Raman spectroscopy is that its spatial resolution is limited by the spot of the laser itself and that a significant volume of material must be probed to obtain an adequate SNR. This is the reason for performing confocal Raman spectroscopy on the coffee-ring, in order to have the massive presence of vesicles and thus a sufficient amount of material to obtain a good SNR. Conversely, TERS



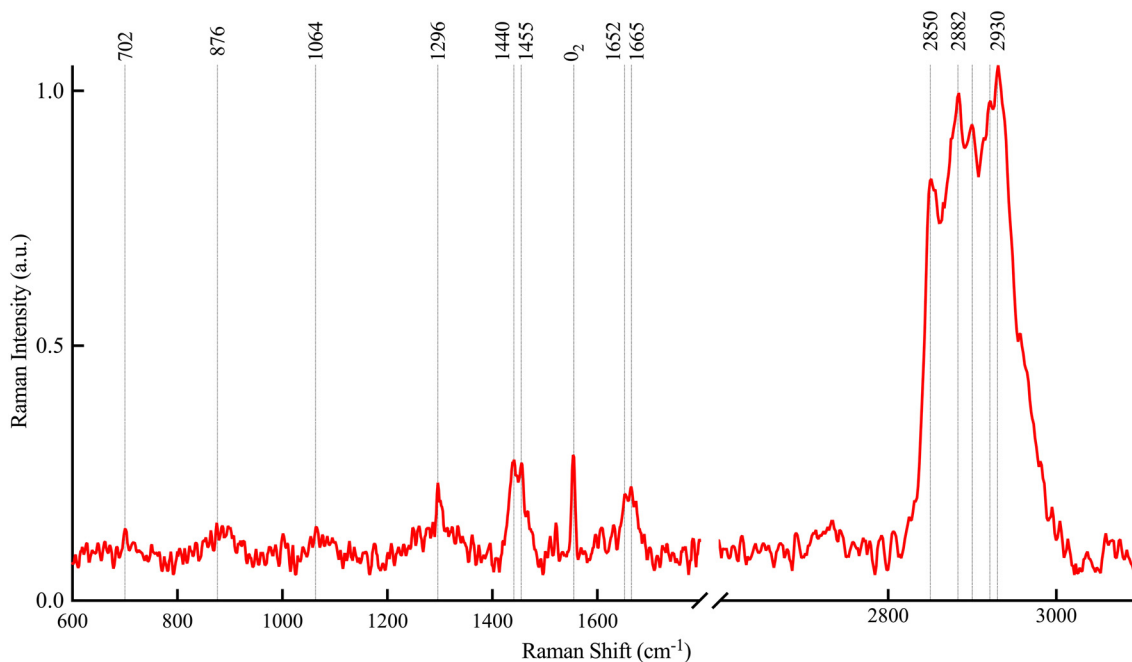


Fig. 4 Example of a TERS spectrum acquired on mEVs.

has generally a poorer SNR because the enhancement of the electromagnetic field due to the tip allows one to collect the signal from a nanometer-sized volume. So, notwithstanding the plasmonic amplification, only a smaller volume of the sample contributes to the signal resulting in a lower SNR. Nevertheless, this allows TERS to probe the sample with nanometer spatial resolution, which makes it suitable for nanoscale measurements, *e.g.*, not enabling the study of the average properties of a huge amount of mEVs as confocal Raman spectroscopy, but allowing the investigation of a single EV. In turn, this would enable one to assess the variation of the properties among the various vesicles of the population and to investigate the variation of the chemical properties on the surface of a vesicle. In the following, this possibility of probing a single EV in different locations is explored.

#### TERS characterization of a single mEV

The potentiality of TERS in the analysis of mEVs in terms of spatial resolution was demonstrated by selecting an isolated mEV and probing different locations on its surface. The study was focused in particular on the signal corresponding to the CH stretching as it resulted in the peaks with the highest intensity. Therefore, the analysis was limited to the range 2750–3050  $\text{cm}^{-1}$ . Fig. 5(a) shows a typical isolated mEV. On the basis of its size, it can be considered representative of typical mEVs. Different spectra were collected in correspondence with 9 points on the surface, indicated with letters from (a) to (i) in Fig. 5(b), using 2.5 mW power, 3 s exposure time and 4 accumulations. The limitation to 9 points was ascribed to the presence of thermal drift (particularly overheating by the laser impacting the sample), which, by increasing the temperature

of the sample, causes the zone of interest to shift (*i.e.*, a single vesicle might shift a few hundred nm and cause the analysis to be performed on the substrate or on totally different zones). In order to solve this problem, it is therefore necessary to limit the duration of the analysis (*i.e.*, the number of points) and the power that impacts the sample, thus limiting the temperature rise and hence the thermal drift.

The spectra acquired in correspondence with the 9 points selected on the surface have been averaged obtaining the spectrum reported in Fig. 5(c), which is characterized by the presence of three more intense peaks at 2882, 2906 and 2930  $\text{cm}^{-1}$ . Really, in the case of biological materials, the analyzed spectral region is characterized by an abundance of peaks which therefore are difficult to rationalize. As for the two peaks at 2882 and 2930  $\text{cm}^{-1}$ , they can be attributed to  $\text{CH}_2$  and  $\text{CH}_3$  stretching, as already found using standard Raman spectroscopy. Nevertheless, when analyzing the single spectra obtained at different points, a higher number of peaks can be detected. Indeed, the fitting procedure (carried out using Origin2021 Pro) indicated an average of 15 peaks in each collected spectrum. Differences among the collected spectra indicate the dependence of the Raman signal on the actual location of the mEV probed using the plasmonic tip. This demonstrates the capability of TERS to detect differences in the chemical composition of mEVs with nanometer lateral resolution. The main information from this technique is related to the surface of the sample (the very first few nanometers on the sample) so, ideally, only the signal from the lipid membrane is observed and, thanks to the correlation with the topographic information, highly spatially resolved structural and chemical information can be obtained. Nonetheless, the identification of



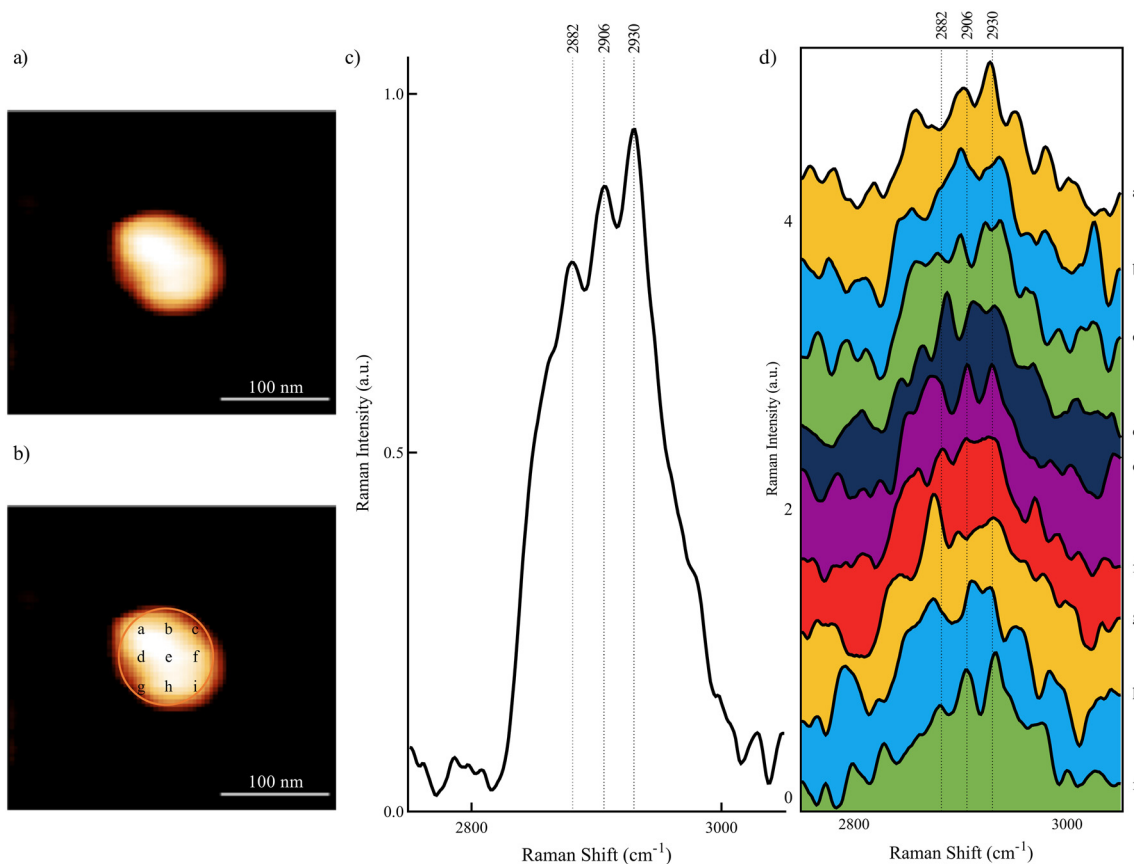


**Fig. 5** (a) Image of a typical mEV and (b) the same mEV image where 9 different points of the surface were probed, indicated with letters from (a) to (i); (c) average spectrum obtained in the range of 2750–3050  $\text{cm}^{-1}$  from the acquired 9 spectra which are reported in (d).

specific organic compounds from the local Raman spectrum is very difficult as the accurate assignment of the detected peaks is hampered by the high number of molecules which present peaks in the CH stretching zone. The accurate rationalization of the acquired spectra, however, would require a deeper analysis which far exceeds the scope of this study. Limiting the analysis to the peaks ascribable to the  $\text{CH}_2$  and  $\text{CH}_3$  bonds (2882 and 2930  $\text{cm}^{-1}$ , respectively), it is possible to demonstrate the capability of nanoscale chemical mapping on single mEVs of TERS. As an example, Fig. 6 shows the variation of the intensity of the two peaks at 2882 and 2930  $\text{cm}^{-1}$  in correspondence with some of the investigated points. In correspondence with point d in Fig. 6, the intensity of the peak at 2882  $\text{cm}^{-1}$  was 10% higher than that of the peak at 2930  $\text{cm}^{-1}$ . In other points the two peaks have almost the same intensity. Finally, in some points like (a) or (i) the intensity of the peak at 2882  $\text{cm}^{-1}$  is about 50% of that of the peak at 2930  $\text{cm}^{-1}$ . This can be associated with a non-uniformity in the distribution of  $\text{CH}_2$  and  $\text{CH}_3$  bonds on the surface, which seems to suggest a certain heterogeneity of the mEV surface at the nanoscale. Also, it is worth noting that the possibility to localize certain functional groups on the mEV surface also depends on the dimension of the volume of the material from which the local Raman signal is collected which limits the lateral resolution of the technique.

A too large volume of material experiencing the plasmonic amplification of the TERS signal would result in a cross-talk among the Raman signal from two adjacent locations reducing the sensitivity and resolution of the method. On the basis of the nominal radius of the tip used in this study, a negligible cross-talk among the adjacent points in Fig. 6 should be expected. Nevertheless, the increase in the radius of the tip due to wearing and melting because of the prolonged exposure to the laser radiation could reduce the actual resolution of the technique. More detailed studies would be needed to address this issue and quantify the actual resolution of the method. Also, while this study demonstrated the capability of TERS to detect specific molecular bonds on the surface of a single mEV, the possibility of identifying specific molecules depends on their actual characteristic Raman peaks. In particular, in the present study, a variation of the  $\text{CH}_2$  and  $\text{CH}_3$  bonds has been revealed, without the possibility of assigning this variation to the distribution of specific molecules.

The capability to select the location of the sample to analyse represents a relevant advantage of TERS. Indeed, in principle, Raman and TERS characterization studies can be dramatically affected by artifacts from the substrate, residuals of chemicals, or possible contaminants, which may result in the presence of spurious peaks in the same spectral region where the samples under investigation have their characteristic



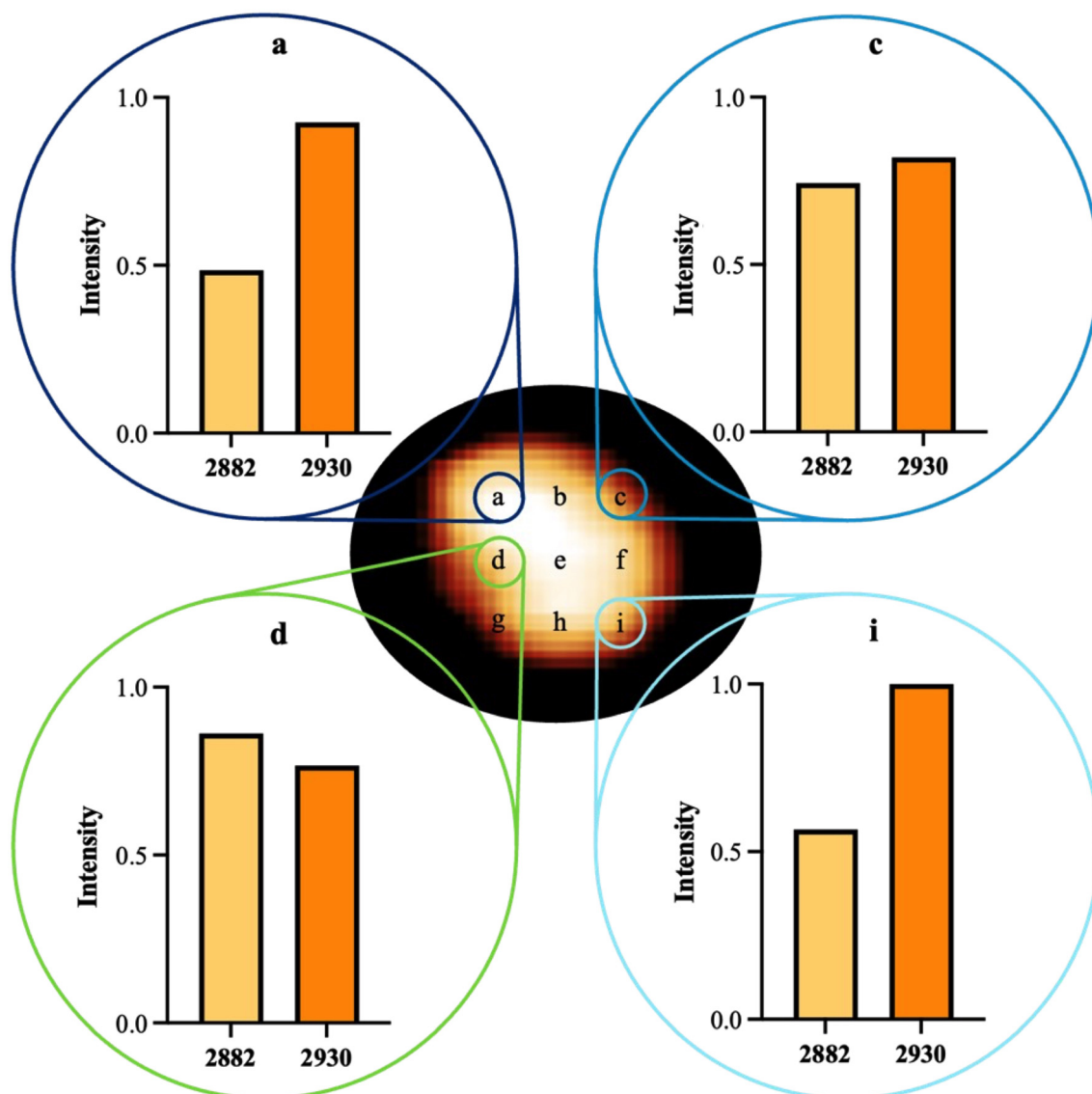


Fig. 6 Variation of the intensity of the TERS peaks at  $2882\text{ cm}^{-1}$  and  $2930\text{ cm}^{-1}$ , which are associated with  $\text{CH}_2$  and  $\text{CH}_3$  bonds, on four nanosized regions of the surface of the mEV.

peaks and bands. Actually, this is the reason for the choice of the  $\text{CaF}_2$  substrate instead of glass ones. Also, the possible presence of spurious peaks induced by residuals of PBS, in which mEVs were kept after isolation, should be discussed. In fact, from a practical point of view, in our experiment the presence of PBS can be considered marginal as the sample, before being deposited on the slide, was also further diluted with distilled water. However, a preliminary Raman investigation of bare PBS was performed. When still in solution, no features were coherently present in the Raman spectrum due to the fact that the salts are dissociated. Due to the evaporation of water, salt crystals start to form on the sample. When acquiring the Raman spectrum in correspondence with massive residuals of PBS after drying, the contribution to the spectrum of PBS is generally negligible. The only region in which it may be significant is a broad band between  $800\text{ cm}^{-1}$  and  $1000\text{ cm}^{-1}$ .

Notably, in this region, mEVs show clear and narrow peaks which cannot be confused with those of PBS. Moreover, the band in the PBS spectrum is more intense between  $900\text{ cm}^{-1}$  and  $1000\text{ cm}^{-1}$ , where mEVs do not show peaks. Moreover, when performing Raman analysis on micrometer-sized crystals, only a weak peak is observed closely below  $1000\text{ cm}^{-1}$  which can be identified as corresponding to the  $\text{HPO}_4^{2-}$  ion at  $989\text{ cm}^{-1}$ .<sup>34</sup> Actually, due to the dimension of the size of the laser beam, some crosstalk may also be present when analysing the points of the sample near the microcrystals. Conversely, as far as TERS spectra are regarded, it must be noted that they show characteristic peaks in the range  $1300\text{--}1700\text{ cm}^{-1}$  and in the range  $2800\text{--}3000\text{ cm}^{-1}$  where no contribution from PBS was observed. Indeed, this is due to the fact that the high lateral resolution of TERS allowed us to probe areas of the mEV sample where PBS residuals were not





present. This confirms that one of the main advantages of TERS is that it allows one to perform local Raman spectroscopy at selected locations of interest of the sample. Therefore, such spectra can be selectively obtained on the samples of interest (*e.g.*, the mEVs in the present work) avoiding residuals and other not interesting materials as they can be clearly distinguished in optical microscopy (if relatively big) or AFM images (if at the submicron scale).

Enabling one to perform Raman spectroscopy at selected points of the sample with nanometer lateral resolution, TERS is virtually capable of extending the application of Raman spectroscopy at the nanoscale. In the specific case of EVs, of which mEVs are an example, Raman spectroscopy has been proposed as a tool to study populations and subpopulations of extracellular vesicles derived from different biological sources, *e.g.*, to assess their purity or for diagnostic purposes.<sup>10,35–43</sup> While confocal Raman spectroscopy involves the global analysis of the mean properties of a large number of vesicles, TERS may enable the investigation of single EVs with high spatial resolution, *e.g.*, to identify domains and specific fingerprint areas to be used as biomarkers. Also, using the approach described, TERS could be used to characterize and map proteins or lipids on the surface of single vesicles. Indeed, on the lipid membrane which constitutes the surface of extracellular vesicles there are plenty of molecules (including not only lipids, but also proteins, nucleic acids, and glycans), the variety of which reflects and may be used to identify the cell of origin and its activity.<sup>44</sup> Among the different EVs, the biochemical analysis of milk derived EVs and the description of their lipid and protein content have been recently reviewed.<sup>45</sup> In fact, Raman spectroscopy has been extensively used in the study of both proteins<sup>46</sup> and lipids.<sup>28</sup> Therefore, it is quite natural to use TERS to extend such analysis to the nanometer scale. Indeed, TERS has been proposed to analyze the protein structure.<sup>16,47–49</sup> The possibility to study proteins in a complex structure like the membrane of extracellular vesicles, however, requires the capability to acquire local TERS spectra with a sufficient SNR where characteristic peaks can be univocally identified. In other words, the prerequisite for the profiling of proteins on the EV surface is the capability to obtain a Raman spectrum to be used as the ‘fingerprint’ of a certain protein. Nevertheless, obtaining such a degree of information at the nanoscale could dramatically improve the knowledge of the properties of EVs in view of possible applications, *e.g.*, in the biomedical field.<sup>20</sup>

Overall, the reported results demonstrated that TERS may represent a powerful technique to analyze the surface of EVs by acquiring complete local Raman spectra and mapping the variation of intensity of the relevant peaks. Indeed, the latter corresponds to variations in the quantity of the molecules corresponding to those characteristic peaks, allowing one to map variations in the chemical composition on the surface of the sample. Such images should reflect – qualitatively or semi-quantitatively, *i.e.*, referring to the relative composition – the distribution of a certain molecule or a certain group on the surface of the EVs. Notwithstanding these promising opportu-

nities, the routine and standardized application of TERS is currently limited by the spatial resolution of the technique, due to the radius of the coated tip, by the need for a higher SNR which must be obtained avoiding nevertheless too intense and prolonged exposure to the laser radiation to avoid heating and degradation of the sample, as well as by the drift of the instrumentation when the nanometer spatial resolution is required. Notwithstanding these limitations, the results of this study confirm that TERS can effectively resolve the heterogeneity in the chemical composition of single mEVs and in particular of their membrane at the nanometer scale, making this technique promising for advanced studies, *e.g.*, to investigate the mechanisms of loading of mEVs at the molecular scale.

## Conclusions

In conclusion, TERS has been demonstrated as a powerful tool to investigate the chemical analysis of mEVs and, more in general, of EVs at the nanometer scale at the level of a single vesicle. After obtaining standard Raman spectra on an extended area of mEVs to be used as their reference ‘signature’, TERS has been performed on the same area in order to assess its capability to identify the characteristic peaks. Then, variations in the distribution of specific bonds, *i.e.*, CH<sub>2</sub> and CH<sub>3</sub>, on the surface of a single mEV selected on the sample have been analyzed confirming the capability of TERS to perform chemical mapping at the nanoscale on the surface of single EVs.

## Author contributions

LB, AP, and DP designed the work. LB isolated the mEVs using the protocol set up with the support of ST and LD and prepared the samples for TEM and AFM analyses. MR provided the instrumental facilities. FM performed TEM analysis. LB performed AFM analysis and analyzed the morphological data. AP, LB, GLP, and CM performed TERS analysis. AP, LB, and GLP analyzed the TERS results. MR and DP supervised the work. LB and AP were the major contributors in writing the first draft of the manuscript, which was revised by DP and then revised and approved by all the authors.

## Conflicts of interest

The authors declare that they have no competing interests.

## Acknowledgements

This work was partially supported by the Sapienza University of Rome through the grants Progetti di Ricerca 2020 (project: STAGES, protocol number RM120172B479E2E8) and Progetti di Ricerca 2021 (project: MENS, protocol number RM12117A81FD8EE0).



## References

- 1 S. Mecocci, M. Trabalza-Marinucci and K. Cappelli, *Animals*, 2022, **12**, 3231.
- 2 L. Cheng and A. F. Hill, *Nat. Rev. Drug Discovery*, 2022, **21**, 379–399.
- 3 J. Munir, A. Ngu, H. Wang, D. M. O. Ramirez and J. Zempleni, *Pharm. Res.*, 2023, **40**, 909–915.
- 4 X. Feng, X. Chen, X. Zheng, H. Zhu, Q. Qi, S. Liu, H. Zhang and J. Che, *Front. Nutr.*, 2021, **8**, 855.
- 5 M. Y. Tian, D. X. Hao, Y. Liu, J. He, Z. H. Zhao, T. Y. Guo, X. Li and Y. Zhang, *Food Funct.*, 2023, **14**, 1320–1337.
- 6 M. Imanbekova, S. Suarasan, Y. Lu, S. Jurchuk and S. Wachsmann-Hogiu, *Nanophotonics*, 2022, **11**, 2827–2863.
- 7 Y. Kwon and J. Park, *Micro Nano Syst. Lett.*, 2022, **10**, 1–13.
- 8 R. R. Jones, D. C. Hooper, L. Zhang, D. Wolverson and V. K. Valev, *Nanoscale Res. Lett.*, 2019, **14**, 1–34.
- 9 G. Pezzotti, *J. Raman Spectrosc.*, 2021, **52**, 2348–2443.
- 10 A. Gualerzi, S. A. A. Kooijmans, S. Niada, S. Picciolini, A. T. Brini, G. Camussi and M. Bedoni, *J. Extracell. Vesicles*, 2019, **8**, 1568780.
- 11 J. Zini, H. Saari, P. Ciana, T. Viitala, A. Löhmus, J. Saarinen and M. Yliperttula, *Eur. J. Pharm. Sci.*, 2022, **172**, 106135.
- 12 W. Lee, A. Nanou, L. Rikkert, F. A. W. Coumans, C. Otto, L. W. M. M. Terstappen and H. L. Offerhaus, *Anal. Chem.*, 2018, **90**, 11290–11296.
- 13 C. F. Morasso, D. Sproviero, M. C. Mimmi, M. Giannini, S. Gagliardi, R. Vanna, L. Diamanti, S. Bernuzzi, F. Piccotti, M. Truffi, O. Pansarasa, F. Corsi and C. Cereda, *Nanomedicine*, 2020, **29**, 102249.
- 14 M. Fleischmann, P. J. Hendra and A. J. McQuillan, *Chem. Phys. Lett.*, 1974, **26**, 163–166.
- 15 Z. Zhang, S. Sheng, R. Wang and M. Sun, *Anal. Chem.*, 2016, **88**, 9328–9346.
- 16 S. Bonhommeau, G. S. Cooney and Y. Huang, *Chem. Soc. Rev.*, 2022, **51**, 2416–2430.
- 17 D. Mrdenović, W. Ge, N. Kumar and R. Zenobi, *Angew. Chem., Int. Ed.*, 2022, **61**, e202210288.
- 18 D. Mrdenović, Z. X. Tang, Y. Pandey, W. Su, Y. Zhang, N. Kumar and R. Zenobi, *Nano Lett.*, 2023, **23**, 3939–3946.
- 19 K. F. Gibson, S. G. Kazarian and S. S. Kharintsev, *Encycl. Anal. Chem.*, 2019, pp. 1–33.
- 20 T. Stepanenko, K. Sofińska, N. Wilkosz, J. Dybas, E. Wiercigroch, K. Bulat, E. Szczesny-Malysiak, K. Skirlińska-Nosek, S. Seweryn, J. Chwiej, E. Lipiec and K. M. Marzec, *Analyst*, 2024, **149**, 778–788.
- 21 L. Tong, H. Hao, X. Zhang, Z. Zhang, Y. Lv, L. Zhang and H. Yi, *Mol. Nutr. Food Res.*, 2020, **64**, 1901251.
- 22 L. Tong, S. Zhang, Q. Liu, C. Huang, H. Hao, M. S. Tan, X. Yu, C. K. L. Lou, R. Huang, Z. Zhang, T. Liu, P. Gong, C. H. Ng, M. Muthiah, G. Pastorin, M. G. Wacker, X. Chen, G. Storm, C. N. Lee, L. Zhang, H. Yi and J. W. Wang, *Sci. Adv.*, 2023, **9**, 15.
- 23 K. Blans, M. S. Hansen, L. V. Sørensen, M. L. Hvam, K. A. Howard, A. Möller, L. Wiking, L. B. Larsen and J. T. Rasmussen, *J. Extracell. Vesicles*, 2017, **6**, 1294340.
- 24 A. N. Böing, E. van der Pol, A. E. Grootemaat, F. A. W. Coumans, A. Sturk and R. Nieuwland, *J. Extracell. Vesicles*, 2014, **3**, 23430.
- 25 A. Lucia, O. A. Cacioppo, E. Iulianella, L. Latessa, G. Moccia, D. Passeri and M. Rossi, *Appl. Phys. Lett.*, 2017, **110**, 103105.
- 26 A. Gualerzi, S. Niada, C. Giannasi, S. Picciolini, C. Morasso, R. Vanna, V. Rossella, M. Masserini, M. Bedoni, F. Ciceri, M. E. Bernardo, A. T. Brini and F. Gramatica, *Sci. Rep.*, 2017, **7**, 1–11.
- 27 Z. Movasaghi, S. Rehman and I. U. Rehman, *Appl. Spectrosc. Rev.*, 2007, **42**, 493–541.
- 28 K. Czamara, K. Majzner, M. Z. Pacia, K. Kochan, A. Kaczor and M. Baranska, *J. Raman Spectrosc.*, 2015, **46**, 4–20.
- 29 V. Mangolini, A. Gualerzi, S. Picciolini, F. Rodà, A. Del Prete, L. Forleo, R. A. Rossetto and M. Bedoni, *Biology*, 2023, **12**, 227.
- 30 J. Penders, A. Nagelkerke, E. M. Cunnane, S. V. Pedersen, I. J. Pence, R. C. Coombes and M. M. Stevens, *ACS Nano*, 2021, **15**, 18192–18205.
- 31 S. G. Kruglik, F. Royo, J. M. Guigner, L. Palomo, O. Seksek, P. Y. Turpin, I. Tatischeff and J. M. Falcón-Pérez, *Nanoscale*, 2019, **11**, 1661–1679.
- 32 J. Zini, H. Saari, P. Ciana, T. Viitala, A. Löhmus, J. Saarinen and M. Yliperttula, *Eur. J. Pharm. Sci.*, 2022, **172**, 106135.
- 33 M. R. Philpott, *J. Chem. Phys.*, 1975, **62**, 1812–1817.
- 34 M. D. Fontana, K. Ben Mabrouk and T. H. Kauffmann, *Spectrosc. Prop. Inorg. Organomet. Compd.*, 2013, **44**, 40–67.
- 35 M. Bukva, G. Dobra, J. Gomez-Perez, K. Koos, M. Harmati, E. Gyukity-Sebestyen, T. Biro, A. Jenei, S. Kormondi, P. Horvath, Z. Konya, A. Klekner and K. Buzas, *Cancers*, 2021, **13**, 1407.
- 36 C. Carlomagno, C. Giannasi, S. Niada, M. Bedoni, A. Gualerzi and A. T. Brini, *Front. Bioeng. Biotechnol.*, 2021, **9**, 640617.
- 37 T. Liangsupree, E. Multia, J. Saarinen, J. Ruiz-Jimenez, M. Kemell and M. L. Riekkola, *Anal. Biochem.*, 2022, **647**, 114672.
- 38 Y. F. Qin, X. Y. Lu, Z. Shi, Q. S. Huang, X. Wang, B. Ren and L. Cui, *Anal. Chem.*, 2022, **13**, 1407.
- 39 H. J. Koster, T. Rojalin, A. Powell, D. Pham, R. R. Mizenko, A. C. Birkeland and R. P. Carney, *Nanoscale*, 2021, **13**, 14760–14776.
- 40 T. T. Bui, E. Jang, J. H. Shin, T. H. Kim, H. Kim, D. Choi, T. D. Vu and H. Chung, *Analyst*, 2023, **148**, 4156–4165.
- 41 Z. Yan, S. Dutta, Z. Liu, X. Yu, N. Mesgarzadeh, F. Ji, G. Bitan and Y. H. Xie, *ACS Sens.*, 2019, **4**, 488–497.
- 42 J. Penders, A. Nagelkerke, E. M. Cunnane, S. V. Pedersen, I. J. Pence, R. C. Coombes and M. M. Stevens, *ACS Nano*, 2021, **15**, 18192–18205.
- 43 W. Lee, A. Nanou, L. Rikkert, F. A. W. Coumans, C. Otto, L. W. M. M. Terstappen and H. L. Offerhaus, *Anal. Chem.*, 2018, **90**, 11290–11296.



- 44 S. Hallal, Á. Túzesi, G. E. Grau, M. E. Buckland and K. L. Alexander, *J. Extracell. Vesicles*, 2022, **11**, e12260.
- 45 S. Buratta, L. Urbanelli, A. Tognoloni, R. Latella, G. Cerrotti, C. Emiliani and E. Chiaradia, *Life*, 2023, **13**, 401.
- 46 A. Rygula, K. Majzner, K. M. Marzec, A. Kaczor, M. Pilarczyk and M. Baranska, *J. Raman Spectrosc.*, 2013, **44**, 1061–1076.
- 47 E. Lipiec, J. Kaderli, J. Kobierski, R. Riek, K. Skirlińska-Nosek, K. Sofińska, M. Szymoński and R. Zenobi, *Angew. Chem., Int. Ed.*, 2021, **60**, 4545–4550.
- 48 S. Bonhommeau, D. Talaga, J. Hunel, C. Cullin and S. Lecomte, *Angew. Chem., Int. Ed.*, 2017, **56**, 1771–1774.
- 49 K. Sofińska, S. Seweryn, K. Skirlińska-Nosek, J. Barbasz and E. Lipiec, *Nanoscale*, 2024, **16**, 5294–5301.

